36th AIAA Plasmadynamics and Lasers Conference AIAA-2005-4657
6 - 9 June 2005, Toronto, Canada

The Optical Environment of a Cylindrical Turret with a Flat Window and the Impact of Passive Control Devices

Stanislav Gordeyev*, Eric J. Jumper†

University of Notre Dame, Notre Dame, IN, 46556

T. Terry Ng‡

University of Toledo, Toledo, OH 43606

Alan B. Cain§

Innovative Technology Applications Company
Chesterfield, Missouri

Optical aberrations over a cylindrical turret with a flat window were measured using a 2-D wavefront sensor and a Malley probe as a function of laser beam elevation angle. It was found that depending on the window back-facing angle the flow either had a weak separation bubble followed by a reattached boundary layer or a strong separation with a large recirculation region behind the cylindrical turret. It was found that optical aberrations were high in the case of a weak separation bubble and at large look-back elevation angles. Different passive devices placed upstream from the turret were studied for their effectiveness in improving the optical-propagation environment. The results are presented and discussed.

I. Introduction

Compressibility effects in turbulent flows at high transonic and supersonic speeds result in non-uniform, highly-unsteady density fields. Changes in density create spatially and temporally varying index-of-refraction fields in the turbulent flow, due to the index-of-refraction dependence on the local density fluctuations ρ',

$$\mathbf{n'(\vec{x},t) = K_{GD}\rho'(\vec{x},t)}, \tag{1}$$

where K_{GD} is the Gladstone-Dale constant and n_0 is the index-of-refraction of media (air). When a collimated laser beam propagates through this field, different portions of the wavefront either advance or retard and the laser beam becomes aberrated. These *aero-optical aberrations*[1] will redistribute laser energy away from the ideal diffraction limited pattern and, in the case of strong aberrations, dramatically decrease the resulting laser intensity on the target thereby reducing the system utility of the beam that may be used for communication, interrogation and targeting or as a directed-energy weapon. The system-performance degradation is usually quantified by examining the far field pattern and quantifying the decrease in the on-axis intensity by computing a Strehl ratio, S_t, as either a function of time or as an average over time. At any given instant the Strehl ratio is given as

$$\mathbf{S_t = \frac{I_t(t)}{I_o}} \tag{2}$$

where I_o is the on-axis, diffraction-limited intensity.

When the laser platform is an aircraft, the two main causes of beam degradation are the thin-layer and immediate air flow around the aircraft, referred to as the *aero-optic* problem[1]; and the intervening,

---

* Assistant Research Professor, Department of Aerospace and Mech. Eng., Member AIAA.
† Professor, Department of Aerospace and Mech. Eng., Fellow AIAA
‡ Professor of Mechanical Engineering.
§ Associate Fellow AIAA, President.

orders-of-magnitude-longer propagation path through the atmosphere to the target, referred to as the *atmospheric-propagation* problem. Since atmospheric effects operate at relatively-low frequencies, they can be mitigated relatively easily with modern beam-control, adaptive-optic methods, when a low-bandwidth deformable mirror compensates these slow aberrations in real time. Aero-optical effects, on the other hand, are consequences of fast changing turbulent flow around an aircraft with typical bandwidth on the order of kHz's, which place it well outside the capabilities of these traditional approaches[2], although the recent development of high-bandwidth wavefront sensors combined with an open-loop control strategy is proving to be a promising direction[3].

Another approach to handle aero-optical problems is to modify the turbulent flow and reduce related optical distortions using passive or active control devices placed upstream of the laser beam's exit pupil (window). In general, relatively-small devices (on the order of the boundary-layer thickness in height) introduce small-scale structures into the incoming boundary layer and modify flow downstream. In a previous paper[4] we showed that small pins and cavities placed upstream from a back-facing ramp reduced optical distortions in the separated flow region over it.

Another type of "passive" flow-control device is one that introduces relatively-large disturbances into the flow just prior to separation. In cases where the flow is strongly separated and forms a fully-separated shear layer over the exit pupil, the cause for the aberrations is the coherent structures that form naturally in the shear layer under the influence of the Kelvin-Helmholtz instability[9]. These structures form roughly along the flow normal direction and are elongated in that direction. It is known that thickening the shear layer can suppress the formation of these coherent structures to some distance downstream over the location they would normally form. Although the exact mechanism responsible for suppressing the formation of spanwise coherent structures in a shear layer by placing various relatively-large devices upstream of separation is uncertain, it is known that they do suppress rollup for extended distances, perhaps by thickening the incoming boundary layer; however, the introduction of these disturbances is known to introduce strong optical aberrations. In the present study, we investigated two configurations of a relatively-large device (see below).

In another previous paper[5] we investigated optically aberrating environment around a generic hemisphere-on-cylinder turret with a flat window at limited elevation and azimuthal angles at several subsonic Mach numbers. It was found that the flow topology and hence the physical mechanism of optical distortions strongly depends on the angle between the window plane and the incoming flow. When the flow over the flat window faces a moderate or strong adverse pressure gradient, it separates. At lowest azimuthal and elevation angles the adverse pressure gradient is localized to the geometric discontinuity at the upstream edge of the window, and the separated flow results in an unsteady separation bubble and subsequent reattached flow over the window. In this case the aberrating character of the flow is identical to that of shallow ramps tested in Ref. 4. When the angle is sufficiently strong to fully separate the flow, the aberrating character of the separated shear layer is identical with that of any of the separated shear layers we have studied previously[9]. Thus, it seems reasonable that devices that have shown promise in improving the optical viewing character for generic aberrating flows over cavities and past ramps should also improve the optical viewing character over a flat-windowed turret.

In order to better understand underlying physics of optical aberrations in the separated region over the windows of flat-windowed turrets, a simpler experiment with a flat-windowed cylindrical turret was conducted and is presented here. This approach allowed us to investigate the separated flow over the window and explore a variety of passive control devices placed just upstream of the window in an attempt to reduce optical distortions in an environment similar to that for a three-dimensional turret, but without the more-complicated flow environment present in a three-dimensional configuration that is characterized by horse-shoe vortices at the surface-turret junction and the highly unsteady von-Karman-type wake. Except for the relatively-large devices used in the present study, all the other devices have been previously reported [4]. Thus, prior to describing the cylindrical-turret study, a brief description of the relatively-large device will be given.

Big Vortex Generators. In the present study two configurations of big vortex generators (BVG) were used. This device was first investigated for fully separated flow for flow separating off a backward-facing step of a relatively long cavity. Figure 1 shows a photograph of a device that makes use of four vortex generators. The vortex generators were semi-delta-wing geometry with a 45^{o}-sweep-angle platform and a 1 inch chord at their base. These vortex generators' angles of attack were adjustable and are shown in alternating (or opposite) angle-of-attach configuration, which was found to be the most-effective configuration. Figure 1 also shows the way that the generator-insertion fit into the test section, with the

flow moving from left to right and separating from the lower wall of the tunnel just aft of the generators at the step. The optical axis was normal to the shear layer, as indicated in the figure. In the backward-facing step experiments, the vortex generators were 1 inch apart with the outermost generator being ½ inch from the tunnel walls. With generators set at alternating angles, as shown in Figure 1, the wall "images" simulate an infinite cross-stream row of vortex generators.

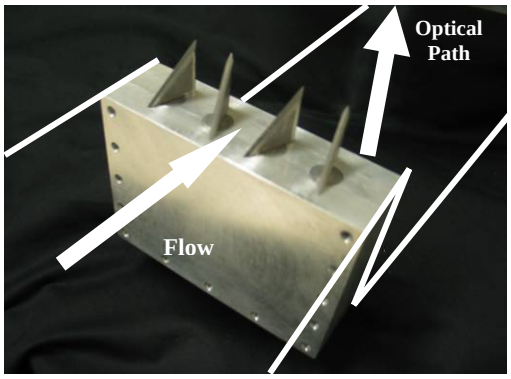

Figure 1. Photograph of the vortex generator device. The lines at the edge indicate how the device was inserted into the test section; the flow entered from the left and the block in which the vortex generators are inserted formed the aft edge of a backward facing step. The vortex generators are placed at alternating opposite angles of attack.

Figure 2 shows an example result, for a 1 μm wavelength beam, of using these relatively-large generators. The generators were set to alternating 20° angles of attack in the manner shown in Figure 1. The approaching flow velocity was M = 0.5. The uppermost pair of figures show the average far-field pattern (left) and frame-to-frame Strehl ratio (right) for the nascent shear layer, absent of any flow-control device, whose OPD_{rms} over the 5 cm aperture was ~0.075 μm; the aperture was centered at 4.5 cm downstream of the separation point. The average far-field pattern is an average of 300 instantaneous far-field patterns constructed from 300 instantaneous, time-uncorrelated, near-field wavefronts, with tilt/tilt removed, over the 5 cm diameter laser beam after propagating normally through the separated shear layer. The middle pair of figures in Figure 2 shows the resulting average far-field pattern and frame-to-frame Strehl ratios with the vortex generators in place. The lower pair of figures in Figure 2 show the dramatic improvement in the Strehl ratio after the 300-frame mean aberration is removed from each frame, increasing the Strehl ratio to ~ 0.98, i.e., essentially diffraction free. The hypothesis is that while vortex generators introduce a disturbance, it is essentially stationary and even a very-low bandwidth adaptive-optic system could probably remove such a disturbance.

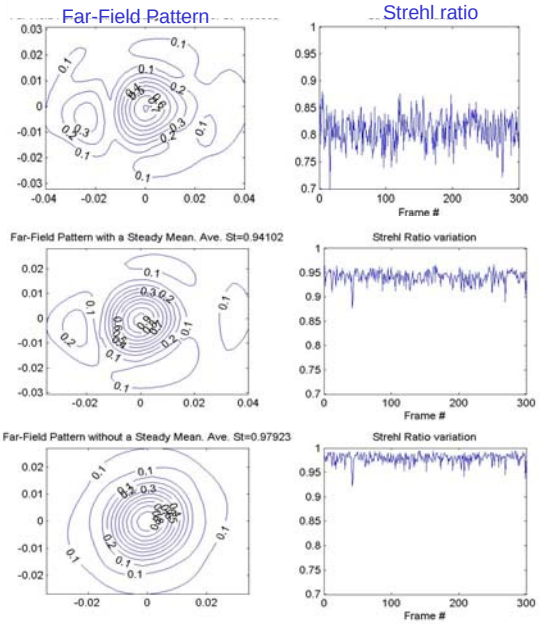

Figure 2. Average Far-Field Pattern (left) and instantaneous Strehl ratio variation for each frame (upper – nascent shear layer, middle - 20° alternating generators, lower – mean OPD removed).

II. Experimental Set-up

All tests were performed in transonic facilities at Hessert Laboratory for Aerospace Research, University of Notre Dame. The facilities were described in detail in Gordeyev at al.[6] and an interested reader is referred to this reference for a complete discussion. The rotating-cylindrical-turret test section was made of optically transparent Plexiglas. A general view and detailed dimensions of the test section with the flat window turret are shown in Figure 3. The rotating cylinder of 4 inches in diameter has a flat window 2 inches long and 3 inches wide with an optically accessible portion of 1.5 inches by 2.5 inches. The cylinder can be rotated to position the flat window relative to the freestream direction at any back-facing angle between 90 and 150 degrees (0 degrees corresponds to the upstream direction). The side wall of the test section is instrumented with 8 steady pressure ports (see top picture in Figure 1) to monitor the streamwise evolution of the flow around the cylinder. Ports are positioned 1" apart along a line on the side wall of the test section 2" from the upper wall. A range of Mach numbers between 0.4 and 0.8 was selected to investigate optical aberrations behind the turret. To achieve these conditions, the flow in the tunnel test section was driven by up to three Allis Chalmer 3,310 CFM vacuum pumps with variable valve settings.

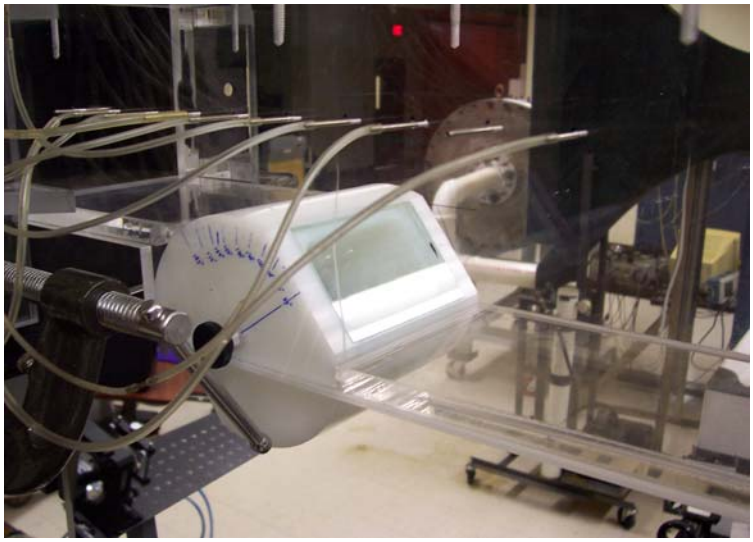

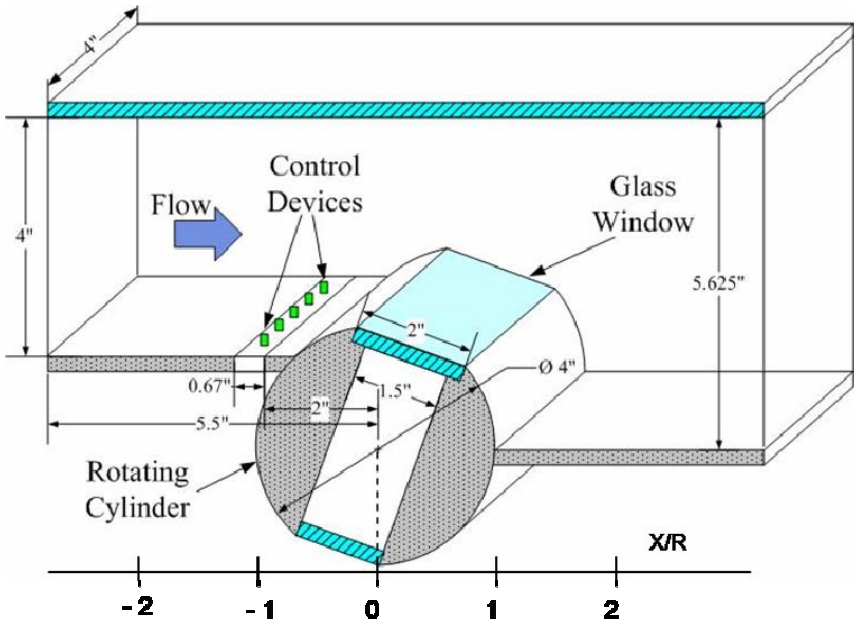

Figure 3. 2-dimensional turret: tunnel model (top) and dimensional drawing (bottom).

In order to measure optical distortions over the flat window two wavefront-measuring instruments were used. The first was a commercially available CLAS-2D 2-dimensional wavefront system. The schematic of the 2-D wavefront optical set-up is presented in Figure 4, left. A circular laser beam 2 inch in diameter was directed through the flat window, normal to it. A return mirror outside of the test section was used to co-axially return the laser beam back to the optical bench. Thus, the beam propagated through the turbulent flow twice, doubling signal-to-noise ratio. The beam's optical distortions were measured using the 2-D Shack-Hartmann wavefront sensor with a 33 x 44 lenselet array mounted in front of the digital camera. The wavefronts were made using a pulsed, frequency doubled Ne-YAG laser with a pulse width of 3 nsec. The wavefronts were sampled at 10 Hz. Several hundred wavefronts were recorded for different elevation angles between 90 and 150 degrees and range of Mach numbers between 0.4 and 0.8. Piston and tip/tilt modes were removed from each wavefront and both the mean and fluctuating parts of the optical wavefronts were computed. Levels of optical distortions were characterized by an average root-mean-square of the fluctuating Optical Path Difference, OPD_{rms}. Note that both tip/tilt and mean lensing effects were removed from OPD_{rms}.

The 2-D wavefront sensor provided spatially resolved wavefronts, but they were totally uncorrelated due to the low sampling rate. To obtain temporal information about the optical distortions over the window, a Malley probe was used. A Malley probe provides continuous time series of one-dimensional slices of wavefronts in the streamwise direction. The probe's principle of operation and detailed description of typical Malley probe set-ups can be found in several papers[4,6,7]. In short, a Malley probe uses two small parallel laser beams (~1mm in diameter) closely positioned (~3-5 mm) in the streamwise direction, see the schematic set-up in Figure 4, right. Instantaneous beam deflection angles are sampled at high rates using an analog Position Sensing Devices (PSD) and 1-D slices of wavefronts can be reconstructed using Taylor's frozen field hypothesis[8]. Also, a Malley probe provides non-intrusive measurements of the convective speeds of optically-aberrating structures in the flow as a function of frequency by computing spectral cross-correlation between two beams[6,7]. In the present set-up, two parallel laser beams were positioned 4 mm apart in the streamwise direction at the center of the flat window insert and deflections angles were recorded using PSD's with the sampling rate of 100 kHz.

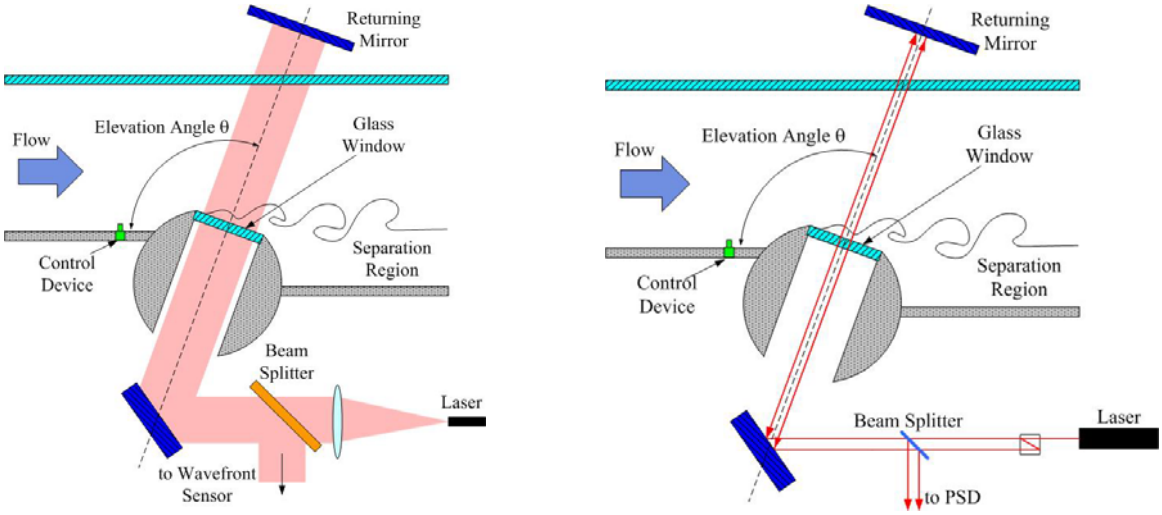

Figure 4. The optical set-up for measuring wavefronts (left) and the Malley probe set-up (right).

In addition to the baseline, several passive control devices were tested for their effectiveness in decreasing unsteady optical distortion over the flat window. Inserts with control devices were placed just upstream of the turret, see Figure 1, bottom. The following devices were tested: spanwise rake of pins with different diameters, small vortex generators (SVG) and big vortex generators (BVG), see Figure 5. Geometrical information is provided in Table 1. It should be noted that all these devices had shown promise in improving the optical-propagation environment when used for flow over a cavity or for flow

separating from a back-facing ramp[4]. All vortex generators were triangular shapes with a 45 degrees leading beveled edge. Heights of pins and small VG's were chosen to be 5 mm, which is on the order of the incoming boundary layer thickness (~7 mm). Two different means of controlling the flow were tested: pins and SVG's, which introduce small scale spanwise distortions into the incoming boundary layer, and BVG's, which produce strong counter-rotating streamwise vortices in the potential flow over and behind the turret.

Table 1. Description of Passive Control Devices

Control Device	Configuration	Height	Spanwise Spacing
Pins, 1 mm	Rake of 1mm vertical cylindrical pins	5 mm	2 mm
Pins, 3 mm	Rake of 3mm vertical cylindrical pins	5 mm	6 mm
Pins, 5 mm	Rake of 5mm vertical cylindrical pins	5 mm	10 mm
Small VG (SVG)	Rake of triangular vertical VG, placed at +/- 30 degrees to incoming flow	5 mm	10 mm
Big VG, Conf 1 (BVG1)	4 triangular vertical VG, placed at +/- 30 degrees to incoming flow	25 mm	50 mm
Big VG, Cong 2 (BVG2)	2 triangular vertical VG, placed at +/- 30 degrees to incoming flow	25 mm	50 mm

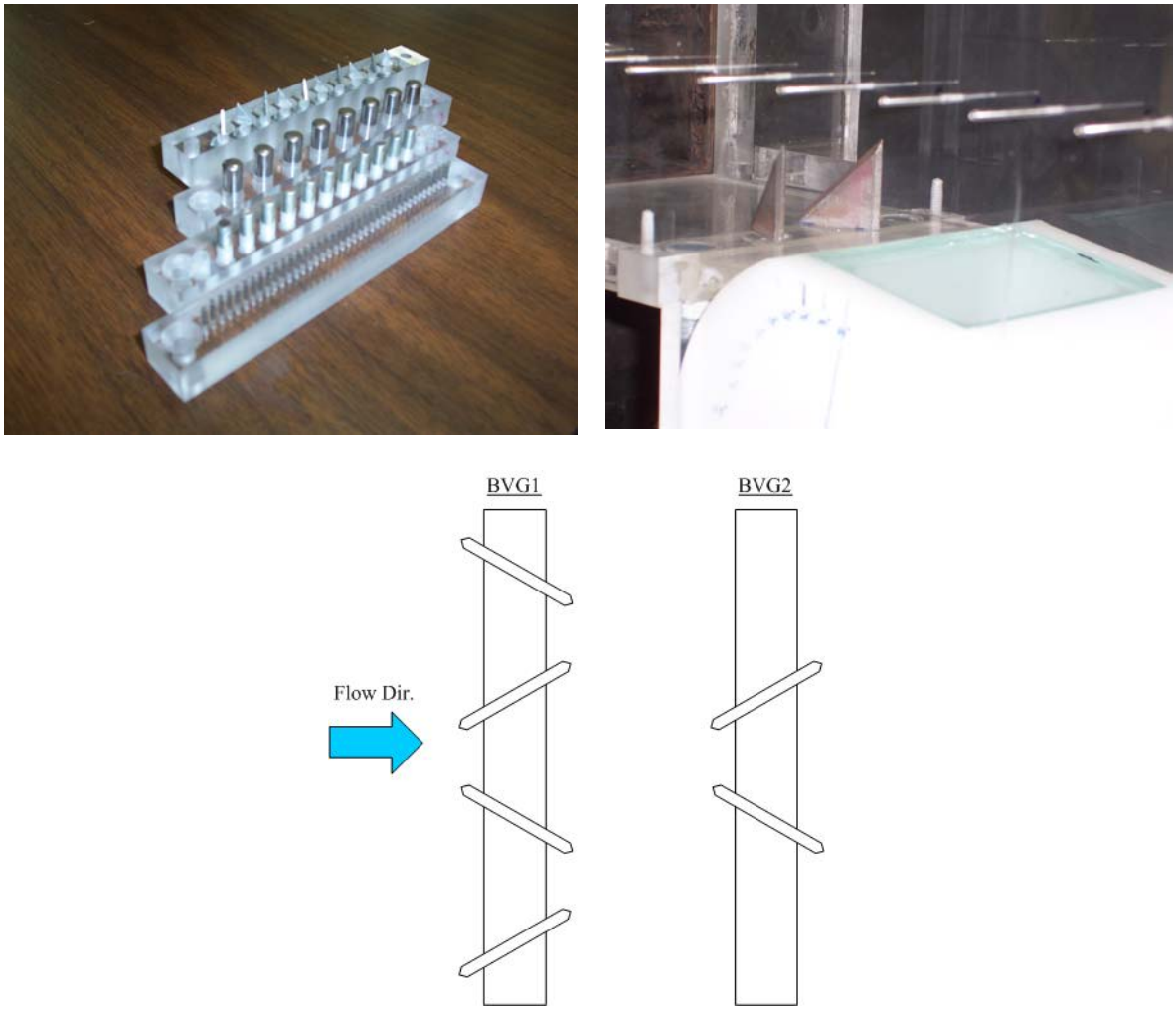

Figure 5. Upper left, Pins and small VG's inserts. Upper right, BVG, Conf 2 (BVG2) installed in the test section. Lower middle, BVG arrangements.

III. Results

A. Baseline.

Mach number distributions along the test section (see Fig. 6) clearly show different flow patterns around the turret for different elevation angles. In the case of the attached flow over the window (92 degree case), the flow did not change significantly in the streamwise direction except a slight deceleration just prior to separating at the downstream edge of the window. In the case of the *weak separation* (100 degree case) the flow accelerates around the turret and over the separation bubble, but re-attaches further downstream on the window. This causes the streamlines to be deflected downward and decreasing the freestream speed downstream of the turret. In the case of the *strong separation* (above 110 degrees), the flow separates at the leading edge of the window and remains separated downstream. For 110 and 120 degrees the initial portion of the cylinder works as a ramp and deflects streamlines upward, causing the freestream Mach number to increase downstream. For elevation angles above 130 degrees the flow separates on the cylinder top. The streamlines therefore stay parallel to the test section walls and Mach numbers don't change downstream. Schematics of the flow topologies for different elevation angles are shown in Figure 7.

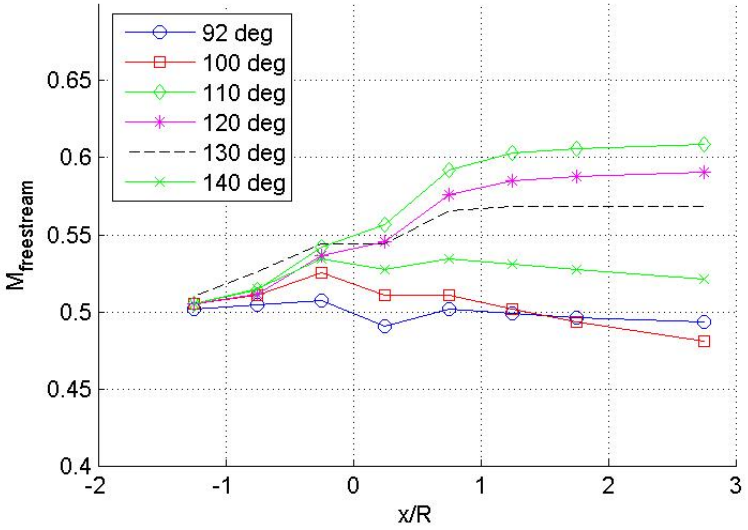

Figure 6. Mach number distribution along the test section at different elevation angles. Incoming M = 0.5.

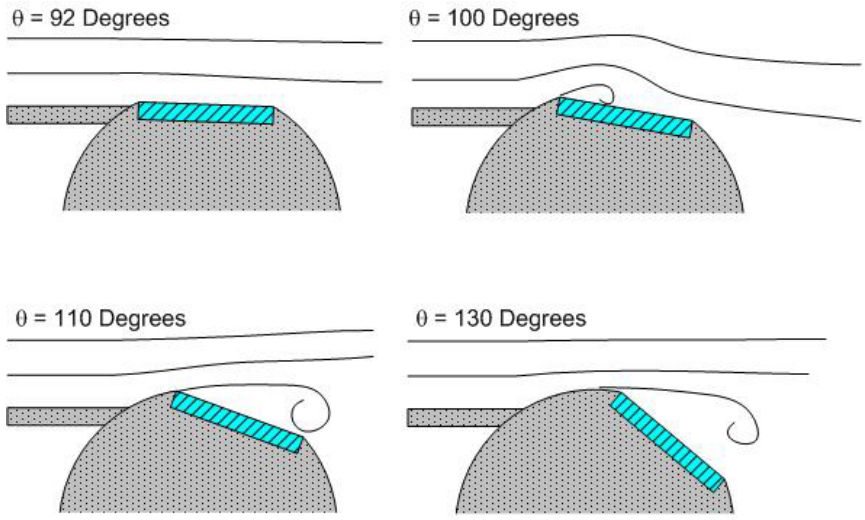

Figure 7. Flow topologies for different elevation angles.

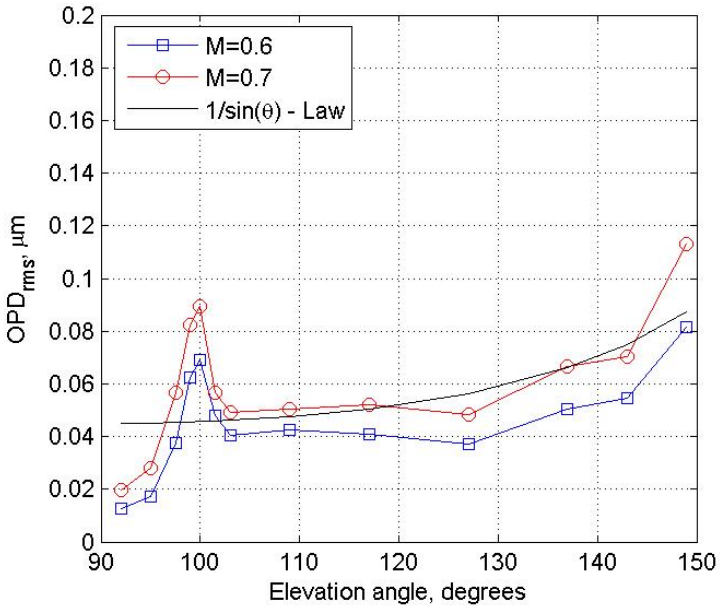

Figure 8. OPD_{rms} as a function of elevation angle at selected Mach numbers.

A summary of baseline (no control devices) optical measurements at two Mach numbers of 0.6 and 0.7 are presented in Figure 8. Since the flow topology varies at different elevation angles, the level of optical distortions strongly depends on the elevation angle. At elevation angles near 90 degrees the flow experiences only a negligible back-facing step and remains attached over the flat window, thus imposing small optical aberrations due to the boundary layer over the window. However, for the elevation angle around 100 degrees the flow experiences a weak separation. An unsteady, small separation bubble is formed at the leading edge of the window. The bubble separates in a non-periodic fashion and is entrained in the reattached boundary layer and is swept over the window. The non-periodic release of coherent structures formed in the separation bubbles have lower-pressure regions inside, which lead to a dramatic increases in optical distortions as can be seen in Figure 8 for elevation angles between 98 and 102 degrees. When the elevation angle increases further, the flow exhibits a strong separation. The separation region extends beyond the window downstream and forms a separated shear layer which originates from the leading edge of the flat window and extends downstream. When the separation bubble is bigger than the window length, its underlying large vortical structure exerts mainly tip/tilt distortions on the laser beam. The distortion are effectively removed from OPD_{rms} data, as described before with smaller aberrations being due to the formation of coherent structures

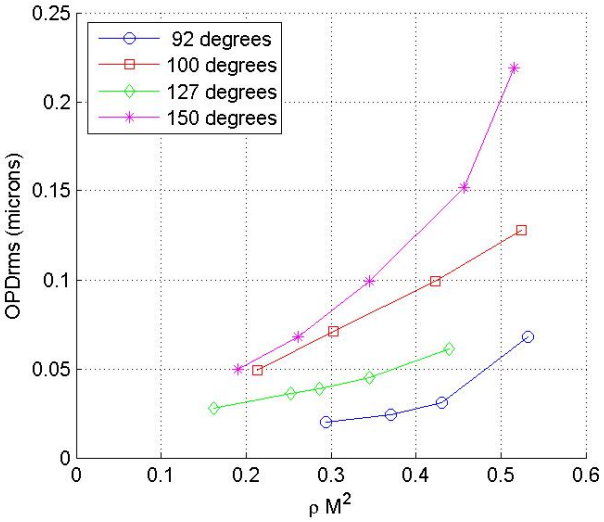

Figure 9. Optical distortions OPD_{rms} as a function of ρM^2 for selected elevation angles.

on the shear layer itself [9]. Therefore the level of optical distortions drops for elevation angles above 100 degrees, see Figure 8. Increasing the elevation angle even further forces the laser beam to go though the separated shear layer at an oblique angle and effectively increases the distance it travels through the region of the turbulent shear layer. From geometrical considerations it follows that optical aberrations should go up as ~1/sin(θ). The experimental data, shown as a solid black line in Figure 8, verify this theoretical trend at least for the measured elevation angles up to 140 degrees. At 150 degrees, however, there is a rise in the curve which might indicate that the shear layer starts growing downstream. This is contrary to the situation at less than 140 degrees where the "1/sin(θ)"-law assumes that the shear layer is approximately the same thickness over the window.

From Figure 8 it can be seen that the Mach number does not affect the OPD dependence on the elevation angles, but simply amplifies the optical aberrations. Optical distortions for a range of Mach numbers are presented in Figure 9 for selected elevation angles. As expected, the optical aberrations follow the trend $OPD_{rms} \sim \rho M^2$, except for high Mach numbers, where local supersonic regions start forming on the cylinder. Dramatic density changes in shocks in supersonic regions greatly increase optical distortions.

B. Passive Control Devices.

When passive devices (like series of pins or small cavities) are placed just upstream of the back-facing ramp, they have been shown to greatly reduce optical aberrations over a 20-degrre back-facing ramp by effectively destroying the 2-dimensional shear layer structure[4]. Due to the similarity in flow physics over the back-facing ramp and the turret with a flat window facing downstream, one might expect that these control devices could also improve the flow and related optical aberrations over the turret. Different passive control devices were placed upstream of the turret and their effects on the flow and the level of optical aberrations were measured. Some of the results are given in Figures 10 and 11.

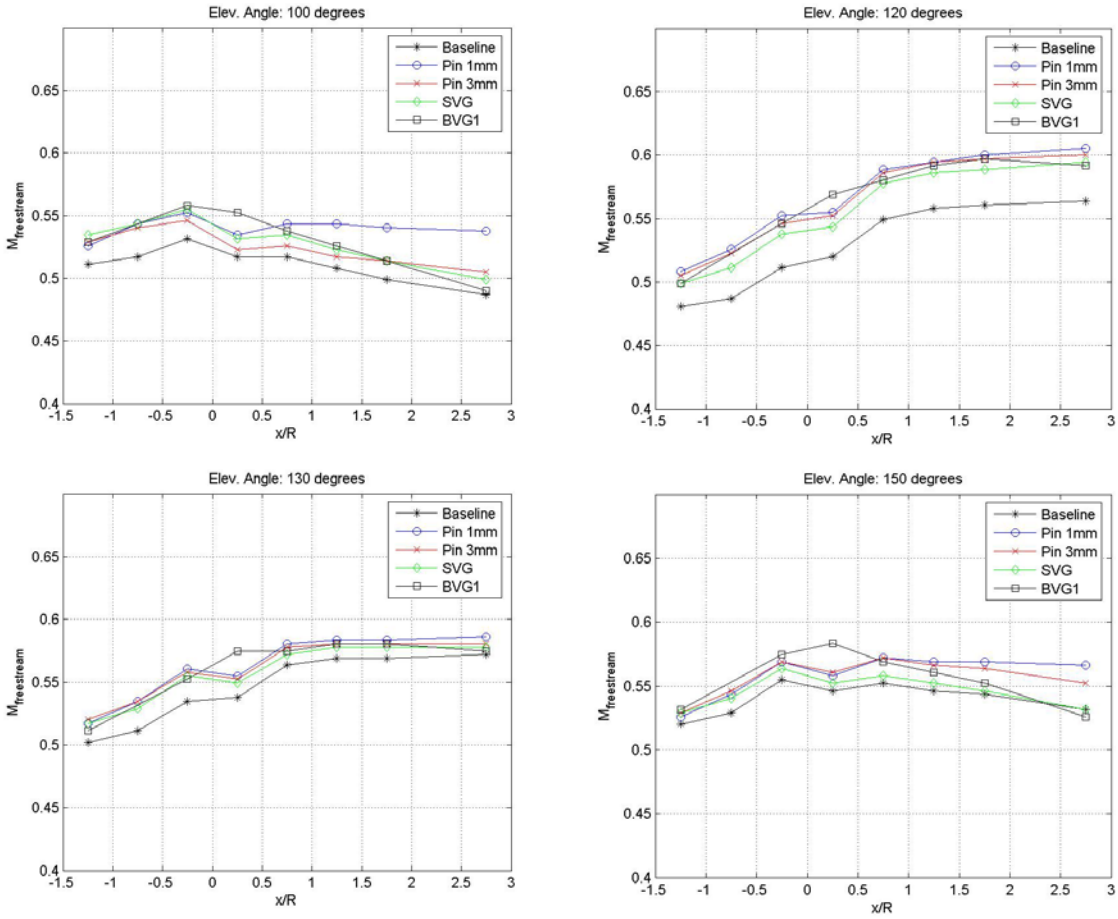

Figure 10. Freestream M streamwise variation for different devices. Incoming M = 0.5.

Pressure Data. Streamwise variation in the freestream Mach number for selected elevation angles and different control devices are presented in Figure 10. As discussed before, the presence of a weak separation bubble and a subsequent re-attachment over the flat insert at 100 degree elevation angle caused the streamlines for the baseline (no device) flow to dip down behind the turret and thus slowing the flow. One-mm pins introduce small scale spanwise structure into the incoming boundary layer and have apparently destroyed the separation bubble and forced a strong separation region to form over the turret, thus resulting in no change in the streamwise Mach number behind the turret (see Figure 10, upper left plot). For elevation angles above 110 degrees, though, the pins do not introduce strong enough disturbances into the boundary layer to modify the potential flow versus the baseline case. Big VG, Conf 1 (BVG1) insert introduces a pair of counter-rotating vortices into the flow with a strong downwash component over the window. These vortices cause the streamlines to dip behind the turret (thus decreasing downstream Mach number) at all elevation angles. This is especially noticeable at 100 and 150 degrees, see Figure 10. A similar, but weaker downwash effect can be seen for the small VG insert.

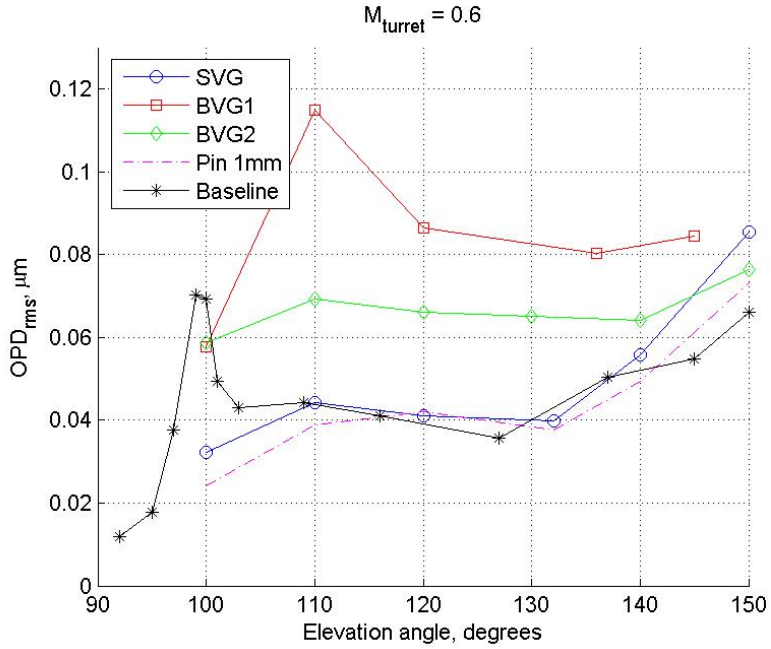

Figure 11. OPDrms vs elevation angle for selected inserts. Mturret = 0.6.

Two-D wavefront optical data, presented as OPDrms with mean and tip-tilt components removed, are shown in Figure 11 as a function of the elevation angle for selected inserts. The Mach number measured at the window insert location (x/R=0.25) and denoted later on as the turret Mach number is 0.6. As discussed before the weak unsteady separation bubble over the flat window at 100 degree elevation angle creates strong density fluctuations over the window, resulting in a spike in OPDrms around 100 degrees. For higher elevation angles the weak separation bubble becomes a strong separation region behind the turret, which imposes mostly tip-tilt distortions and lower, small-scale shear-layer structure aberrations on the laser beam. Since the tip-tilt is removed from the unsteady OPDrms, it leads to a drop in OPDrms above 115 degrees. Once the tip-tilt is removed, the remaining the dominant optical aberration mechanism is the presence of the shear layer over the flat window. For the larger look-back angles, the resulting OPDrms grows as ~1/sin(θ). One-mm pins and small VG effectively disrupt the formation of the weak unsteady separation bubble and dramatically reduce OPDrms at 100 degree elevation angle. For higher elevation angles they do not improve the optical environment, since they do not change the mean potential flow over the turret and therefore the shear layer dynamics downstream of the turret is unchanged. Big VGs do modify the mean flow, but unfortunately introduce additional small-scale vortical structures in the flow especially BVG, Conf. 1 with 4 VG fins (labeled BVG1 in Figure 11). Two-fin BVGs, Conf. 2 (labeled BVG2 in Figure 11), introduce less distortions into the flow but still above that in the baseline case. The

encouraging result is that OPDrms stays flat for the whole range of elevation angles up to 150 degrees, meaning that the "1/sin(θ)"-law is probably disrupted due to the suppression or delaying of vortex merging. A further parametric study of fin positions, sizes and orientations is therefore needed to find the optimum way of modifying the flow around the turret and reducing the optical distortions over the turret.

The mean wavefront results are given in Figure 12. This Figure shows two effects. The strongest is the wake patterns of the vortices formed by the VGs. These wake patterns are caused by the low-pressure, low-density cores of the vortices. The second effect is the mean lensing effect of the curved separated flow. These effects can be clearly seen in Figure 12 for elevation angles 100, 110 and 120 degrees, where OPD is below zero in the vortex wake. VGs are located at -0.01 m and 0.01 m on the horizontal axis, flow goes from bottom to top. Thus, VGs create a strong wake and modify the mean flow and related optical aberrations. For higher elevations the separation region destroys the vortex wake (Figure 10, elevation angle 120 degrees), the VG effect disappears and OPDrms approaches the baseline OPDrms, see Figure 11.

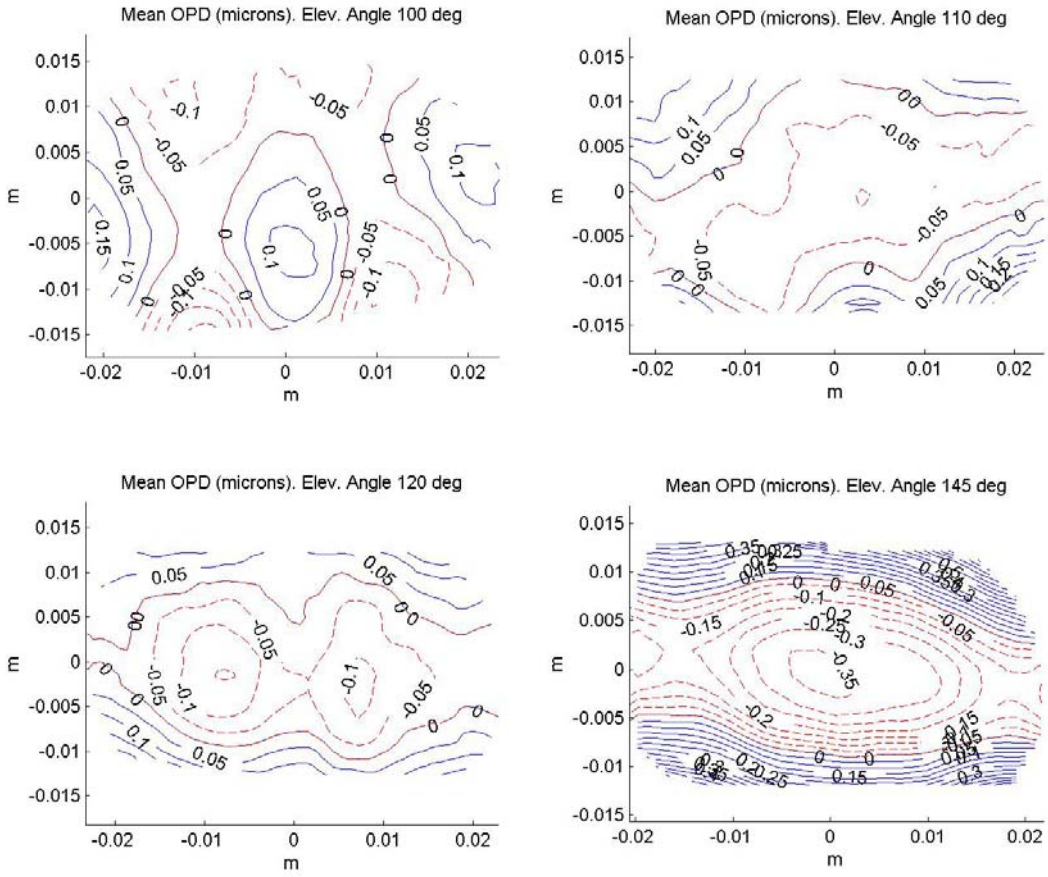

Figure 12. Mean OPD for BVG1 for different elevation angles. M = 0.5. Flow goes from bottom to top.

Convection speed for the optically-active structures were obtained by cross-correlating the Malley probe signals from the probe's two beams in the Fourier domain[6] and signals' power spectra provided information about structures' scales and intensity. Power spectra for the base flow and selected devices at several elevation angles are shown in Figure 13. Tunnel mechanical vibrations are responsible for sharp peaks below 1 kHz. Baseline spectra show the presence of broadband peak around 4kHz for all elevation angles. Baseline spectra grow in intensity for high elevation angles, which is consistent with the baseline OPDrms increase in Figure 11.

One-mm pins introduce small scale structures into the boundary layer and, at 110-130 degrees, tend to shift the peak in spectra toward higher frequencies of 6-10 kHz without modifying the lower frequency part. One exception is the 150 degree case, where low-frequency part of spectra is reduced below the baseline (see Figure 13 lower right plot). While the 1-mm pins suppress low-frequencies, they do add

high-frequency content (above 10kHz). The resulting optical distortion is thus about the same as in the baseline case.

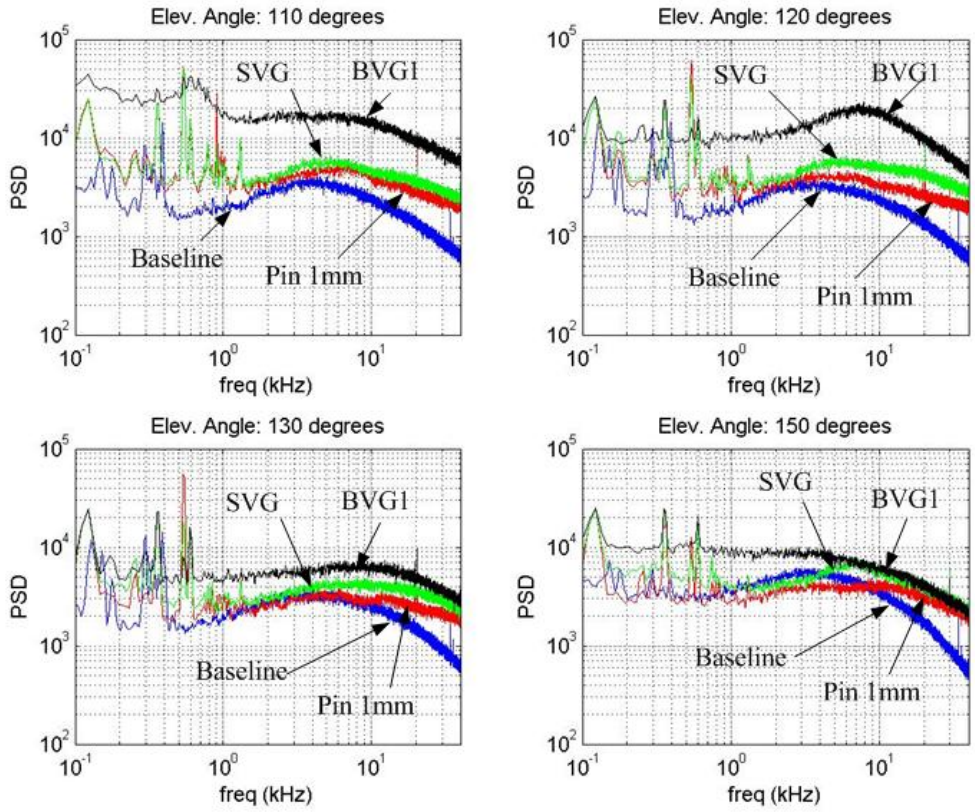

Figure 13. Deflection angles power spectra (PSD) at selected elevation angles. M = 0.5.

Small VGs (labeled SVG in Figure 13) work similarly to 1-mm pins and the associated spectra are very similar to 1-mm pin spectra in Figure 11. This is consistent with wavefront results in Figure 11, where 1-mm pins and SVG produce very similar results.

Four big VG's placed upstream of the turret (labeled BVG1 in Figure 13) introduce strong counter-rotating vortices into the potential part of the flow over the turret, and the vortices interact with the separation region over the turret. The large-scale structure in the wake region is responsible for a hump around 0.7 kHz in the deflection angle spectra at 110 degrees. The structure quickly cascades toward smaller scales and the peak shifts to 7 kHz at 120 degrees and 10 kHz at 130 degrees. By 150 degrees the wake-related structure is destroyed by the separation region behind the turret and the BVG1 spectrum approaches the baseline spectrum (Figure 13, lower right plot).

The slope of the phase-frequency plots for the Malley probe data gives the convective time delay from which the convective speed can be computed for a known beam separation[6]. Phase plots for the baseline case, Pin 1-mm and BVG1 for M_{turret} = 0.5 for elevation angles 100 and 140 degrees are presented in Figure 14. For the baseline case, the aberrating structures move at around 0.6 of the freestream speed behind the turret. Control devices enhance the turbulent mixing and bring high-speed portions of the flow into the separation region. This results in an significant increase in convective speeds, as can be seen in Figure 14 for 1-mm pins (0.9..1.1 of the freestream) and BVG1 (0.85..1.0 of the freestream).

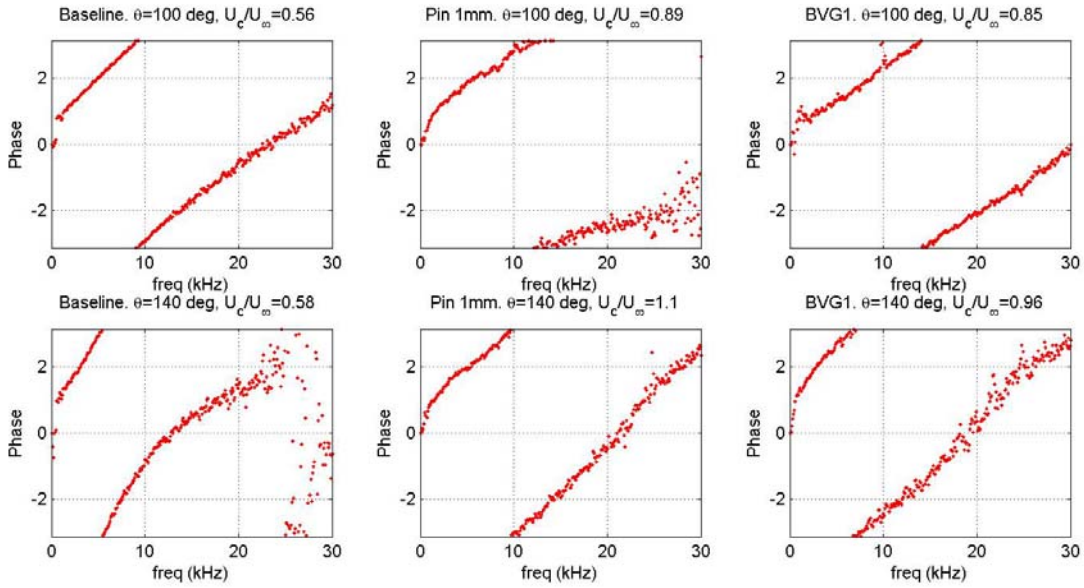

Figure 14. Phase plots from Malley probe for different devices. Mturret = 0.5.

V. Conclusions and Discussions

Optical aberrations over the cylindrical turret with the flat window were measured using both a two-dimensional wavefront sensor and a Malley probe as a function of laser beam/window elevation angle. In the present set of tests, the effects on optical propagation environment of a set of passive flow-control devices were studied. Two classes of devices were studied, each of which showed an improved propagation environment in some situations. The first class is small-disturbance devices and the second the relatively-large disturbance devices. The results in the present study have shown mixed results. First, it is clear that the small devices were effective in improving the viewing environment in the range of elevation angles from 97^o to 105^o; however, the small devices had essentially no effect beyond 110^o and show slightly worse conditions beyond 140^o. On the other hand, the large devices greatly worsened the propagation environment at all angles up to 140^o; however, there were some promising trends demonstrated with the BVG Configuration 2. First, once the mean OPD was removed, although the OPD_{rms} increased by 50% over that of the baseline for elevation angles above 105^o, the propagation environment remained constant out to almost 150^o. In the BVG study briefly described in the *Introduction*, the vortex generators were placed in the immediate vicinity of the separation point. In future studies we will move the location of the vortex generators closer to the leading edge of the window. One could imagine using the small devices at their present locations for elevation angles up to ~ 130^o, then introducing and using BVG-type devices near the leading edge of the window beyond that point while retracting the small devices. Future reporting will address the outcome of such an investigation.

Acknowledgments.

These efforts were sponsored by the Air Force Office of Scientific Research as part of the STTR program in a Phase II effort under contract number FA9550-04-C-0044. Drs. Tom Beutner and John Schmisseur have served as the AFOSR Program Managers. The U.S. Government is authorized to reproduce and distribute reprints for governmental purposes notwithstanding any copyright notation thereon.

References

[1] K. J. Gilbert and L. J. Otten (eds), *Aero-Optical Phenomena*, Progress in Astronautics and Aeronautics, Vol. 80, AIAA, New York, 1982.

[2] Jumper, E.J., and E.J. Fitzgerald, "Recent Advances in Aero-Optics", *Progress in Aerospace Sciences*, **37**, 2001, pp.299-339.

[3] D. Duffin, "Feed-Forward Adaptive-Optic Correction of Aero-Optical Aberrations Caused by a Two-Dimensional Heated Jet", *36th AIAA Plasmadynamics and Laser Conference*, Toronto, Canada, 6-9 Jun, 2005, AIAA Paper 2005-4776.

[4] S. Gordeyev, E. Jumper, T. Ng and A. Cain, "Optical Disturbances Caused by Transonic Separated Boundary Layer Behind a 20-Degree Ramp: Physics and Control", *42nd AIAA Aeroscience Meeting and Exhibit*, Reno, Nevada, 5-8 January, 2004, AIAA Paper 2004-0472.

[5] S. Gordeyev. T. Hayden and E. Jumper, "Aero-Optical and Hot-Wire Measurements of the Flow Around the Hemispherical Turret With a Flat Window", *35th AIAA Plasmadynamics and Laser Conference*, Portland, Oregon, 28 Jun - 1 Jul, 2004, AIAA Paper 2004-2450.

[6] S. Gordeyev, E. Jumper, T. Ng and A. Cain, "Aero-Optical Characteristics of Compressible, Subsonic Turbulent Boundary Layer", *34th AIAA Plasmadynamics and Lasers Conference*, Orlando, Florida, 23-26 June, 2003, AIAA Paper 2003-3606.

[7] Duffin, D. A., Gordeyev, S., and Jumper, E. J., "Comparison of Wavefront Measurement Techniques on a Two-Dimensional Heated Jet," , *35th AIAA Plasmadynamics and Laser Conference*, Portland, Oregon, 28 Jun - 1 Jul, 2004, AIAA Paper 2004-2406.

[8] Malley, M., Sutton, G.W. and Kincheloe, N., "Beam-Jitter Measurements of Turbulent Aero-Optical Path Differences," *Applied Optics*, **31**, pp. 4440-4443, 1992.

[9] Fitzgerald, E.J. and Jumper, E.J., "The Optical distortion mechanism in a nearly incompressible free shear layer, J. Fluid Mech, 512, pp. 153-189, 2004